

Using Neutron Star Observations to Determine Crust Thicknesses, Moments of Inertia, and Tidal Deformabilities

A. W. Steiner,¹ S. Gandolfi,² F. J. Fattoyev,³ and W. G. Newton³

¹*Institute for Nuclear Theory, University of Washington, Seattle, WA 98195*

²*Theoretical Division, Los Alamos National Laboratory, Los Alamos, NM 87545*

³*Department of Physics and Astronomy, Texas A&M University-Commerce, Commerce, Texas 75429, USA*

We perform a systematic assessment of models for the equation of state of dense matter in the context of recent neutron star mass and radius measurements to obtain a broad picture of the structure of neutron stars. We demonstrate that currently available neutron star mass and radius measurements provide strong constraints on moments of inertia, tidal deformabilities, and crust thicknesses. A measurement of the moment of inertia of PSR J0737-3039A with 10% error, without any other information from observations, will constrain the EOS over a range of densities to within 50-60%. We find tidal deformabilities are less than $2.6 \times 10^{36} \text{ g cm}^2 \text{ s}^2$ to 95% confidence, except for neutron stars less massive than 1.4 solar masses. The crustal fraction of the moment of inertia can be as large as 10% for a 1.4 M_\odot permitting crusts to have a large enough moment of inertia reservoir to explain glitches in the Vela pulsar even with a large amount of superfluid entrainment. Finally, due to the uncertainty in the equation of state, there is at least a 40% variation in the thickness of the crust for a fixed mass and radius, implying that future simulations of the cooling of a neutron star crust which has been heated by accretion will need to take this variation into account.

PACS numbers: 26.60.-c, 21.65.Cd, 26.60.Kp, 97.60.Jd

Introduction: Recent neutron star (NS) mass and radius observations have provided new constraints on the neutron star mass-radius curve and on the equation of state (EOS) of dense matter [1]. The EOS, in turn, is a fundamental property of quantum chromodynamics (QCD), probing cold and dense matter which is otherwise difficult to access in experiment.

In the near future, mass and radius observations may be complemented by other constraints on NS structure. While thousands of pulsars have been observed, there is only one binary system where both NSs are radio active pulsars, PSR J0737-3039. The ability to observe pulsations from both NSs and the extreme nature of the system [2, 3], enables a potential measurement of the moment of inertia, I , of one of the neutron stars [4]. Also, the Laser Interferometer Gravitational-Wave Observatory (LIGO) is expected to measure the gravitational wave signal from a NS merger within the near future [5], and a sufficiently large signal to noise observation will enable a measurement of the neutron star tidal deformability [6–10] (denoted by λ and sometimes also called “tidal polarizability”). It turns out these two types of new observations are intimately related: the moments of inertia of a NS is strongly correlated with its tidal deformability [11, 12].

NSs can accrete matter from main-sequence companions which results in the emission of X-rays and the heating of the NS crust. If the accretion stops (referred to as “quiescence” since the X-rays from accretion subside), then the cooling NS crust can be directly observed. The timescale for this cooling is proportional to the square of the NS crust thickness [13], and thus the crust thickness is important for determining the properties of the crust

from observations of crust cooling [14–18].

Another potential constraint of NS structure comes from pulsar glitches. Previous works [19, 20] have shown that, if NS crusts are believed to be the location of the angular momentum reservoir which contributes to the glitch spin up, then a significant fraction of the NS’s moment of inertia must lie in the superfluid component of the crust. Thus glitches are sensitive to the crustal fraction of the moment of inertia, denoted $\Delta I/I$.

Finally, many of these quantities are (at least weakly) correlated with the nuclear symmetry energy [21, 22]. The nuclear symmetry energy is the difference between the energy per baryon of neutron matter and that of nuclear matter (we ignore quartic terms, see Ref. [23]). We denote the symmetry energy, $S(n_B)$, where n_B is the baryon number density, and $S \equiv S(n_0)$ where n_0 is the nuclear saturation density. The quantity $3n_0 S'(n_0)$ is denoted as L . The value of L determines the pressure of neutron-rich matter at the saturation density. The pressure of neutron-rich matter, in turn, is related to all of the above NS structure quantities given above.

For the first time, we use existing NS mass and radius observations to predict the expected ranges of NS properties such as moments of inertia, tidal polarizabilities and crustal thicknesses which are measurable by a diverse range of ongoing observational programs. We generate these expected ranges based on Monte Carlo simulations using parameterizations which explore the full variation which is possible given current uncertainties in the nature of dense matter. Our EOS models are based on recent progress in the microscopic calculation of neutron-rich matter near the nuclear saturation density. At high densities, we assume no additional correlation with mat-

ter at lower densities, and use models which allow for strong phase transitions. Our method is in contrast to several previous works which have computed theoretical predictions of moments of inertia, crust thicknesses, and tidal polarizabilities for smaller samples of representative EOSs [1, 21, 24–31]. Future observations will constitute direct tests of the theoretical framework we use and of the systematics of current mass-radius observations.

Method: For the first observational data set, we use (i) the five mass and radius measurements from photospheric radius expansion bursts in Ref. [32–35] (assuming that the photosphere is extended at “touchdown” as justified in Ref. [33]) and (ii) the five radius measurements from quiescent low-mass X-ray binaries in Refs. [36, 37] taking the hydrogen column densities and distances from the Harris catalog [38] and allowing for either hydrogen or helium atmospheres (this is the choice from Ref. [37] with the largest value for the evidence integral). The second data set additionally assumes a hypothetical 10% measurement of $I = (70 \pm 7) M_\odot \text{ km}^2$ for a $1.338 M_\odot$ NS. The third data set includes only the I measurement and no constraint from other mass and radius observations.

There is a one-to-one correspondence between the NS mass-radius curve and the pressure as a function of energy density, $P(\varepsilon)$. We ensure that all EOSs are causal ($dP/d\varepsilon < 1$), hydrodynamically stable $dP/d\varepsilon > 0$, and also that all mass-radius curves produce a 2 solar mass NS in line with the recent mass measurements in Refs. [39, 40]. Strange quark matter is assumed not to be absolutely stable, so we consider only hybrid NSs where deconfined quark matter is surrounded by a hadronic crust, and leave the consideration of strange quark stars to future work. Moments of inertia are computed using the slowly-rotating (Hartle-Thorne) approximation [41, 42] and we use the correlation in Ref. [11, 12] to compute the tidal deformabilities. We have independently checked this correlation based on the expressions in Refs. [7, 43], and find that the correlation generally holds to within about 1% (since we are ignoring strange quark stars), though slightly larger variations can be generated with strong phase transitions just above the nuclear saturation density. However, such configurations, while not ruled out by the observational data, are finely-tuned and relatively improbable, and thus the results from the correlation are sufficient for our purposes.

There has been significant recent progress [44, 45] on computing the EOS of neutron rich matter from using realistic nuclear forces, both quantum Monte Carlo and using chiral effective theory interactions in many-body perturbation theory. We assume that the binding energy of nuclear matter is -16 MeV, the saturation density is 0.16 fm^{-3} (typical values from Ref. [46]) and employ two different EOSs near the nuclear saturation density. The first is the quantum Monte Carlo model from Ref. [44], and we refer to this model as “GCR”. The limits $12.5 \text{ MeV} < a < 13.5 \text{ MeV}$ and $0.47 < \alpha < 0.53$

are increased slightly from Ref. [47] to ensure that we include all possible models from Ref. [44]. Additionally, we reparametrize b and β in terms S and L . For the second model, we use the parameterization from Ref. [45] (“HLPS”), and the results on neutron matter from Ref. [48] from an interaction based on chiral effective theory. Based on the results from Refs. [49, 50], we choose limits $220 \text{ MeV} < K < 260 \text{ MeV}$. The inferred range on the energy of neutron matter implied by Fig. 1 of Ref. [48] is between 13.5 and 20.1 MeV, implying that the nuclear symmetry energy, S , is between 29.5 and 36.1 MeV. The range on the derivative of the neutron matter EOS is between 95 MeV/fm^3 and 138 MeV/fm^3 , and this implies $44.2 \text{ MeV} < L < 65 \text{ MeV}$. At each point, we fix $\alpha, \gamma, \eta, \alpha_L$, and η_L (see Ref. [45] for their definitions) from K, E_{neut} and E'_{neut} to construct the EOS. For the GCR model, we limit S to between 29.5 MeV and 36.1 MeV as in the HLPS model, and we limit L to be between 30 and 70 MeV which covers the range of L from Ref. [44, 51]. Both nuclear masses and theoretical models imply a correlation between S and L , thus we additionally restrict parameters to lie between $(9.17 S - 266 \text{ MeV}) < L < (14.3 S - 379 \text{ MeV})$ which encloses the constraints from nuclear masses [46], quantum Monte Carlo [44], chiral interactions [48], and isobaric analog states [52] as summarized in Ref. [35]. The GCR and HLPS models are used only up to the nuclear saturation density, as they may not be valid if a phase transition is present. Increasing the density up to which we use these models would improve our constraints on the EOS but does not change the qualitative results. It is particularly critical that we assume no correlation between the EOS near the saturation density and the EOS at higher densities, except for the constraint that $P(\varepsilon)$ is a continuous and monotonically increasing function.

For the NS crust, we use the tabulated crust EOSs based on the work in Ref. [53]. A two-dimensional grid of crust EOSs with varying values of the S and L were computed and this grid was interpolated to generate the crust for general values of S and L in our simulations. For the transition between the crust and the core, we use the correlation between n_t and S and L ,

$$n_t = S_{30} (0.1327 - 0.0898 L_{70} + 0.0228 L_{70}^2) \text{ fm}^{-3} \quad (1)$$

where L_{70} is L in units of 70 MeV and S_{30} is S in units of 30 MeV. For our ranges of S and L , this correlation gives transition densities between 0.06 fm^{-3} and 0.1 fm^{-3} , consistent with those obtained in Ref. [54]. We use this transition density from Eq. 1 to compute the transition pressure, and find values between 0.30 and 0.82 MeV/fm^3 , slightly larger than the range 0.25 to 0.65 MeV/fm^3 found in Ref. [1].

For the EOS above the saturation density, we either use a set of three piecewise polytropes (only five parameters since the transition to the first polytrope is already fixed by the EOS at the saturation density) referred to as

“Model A” in Ref. [34]. Alternatively, we use a set of four line segments in the (ε, P) plane, “Model C” [34]. This latter model is useful because it provides an alternative model which tends to favor stronger phase transitions in the core. The choice of either GCR or HLPS near saturation density and either Model A or Model C at high densities gives a total of four EOS models to use with our three data sets.

For each of the above data sets and EOS models, we perform a Markov chain Monte Carlo simulation as first outlined in Ref. [33]. To obtain our final results for a fixed data set we choose the smallest range which encloses all of the EOS models, as done in Ref. [34]. This procedure is a relatively simple version of a fully hierarchical Bayesian analysis which is currently too computationally expensive.

Results and Discussion: Typically, the HLPS model gives larger NSs than GCR, due to the larger lower limit on L of 44.2 MeV. We also find that Model C gives smaller NSs than Model A, due to the possible presence of phase transitions. Samples from the resulting Markov chains and the confidence limits for quantities of interest for all 12 combinations of data sets are given in the supplementary material.

Currently available mass and radius observations suggest probability distributions for the moment of inertia of a 1.4 solar mass neutron star to as given in the upper left panel of Fig. 1. It is clear that model C, which favors stronger phase transitions gives slightly smaller values for $I(M = 1.4 M_\odot)$ as expected. Among these four models, the smallest 68% lower limit is $61.4 M_\odot \text{ km}^2$ and the largest 68% lower limit is $72.7 M_\odot \text{ km}^2$, i.e. a variation of less than 20%. The corresponding range for the radius of a 1.4 M_\odot NS is 10.6 to 12.1 km, comparable to results obtained previously [33, 34, 37, 47]. The constraint for the $M - R$ data on the pressure at an energy density of 450 MeV/fm³ is 53%. On the other hand, since the systematic uncertainties of currently available mass and radius observations may be larger than that from a future I measurement, it is worth noting that a 10% I measurement alone constrains the pressure to within 55% at that same energy density and to within 59% at an energy density of 1000 MeV/fm³.

Current mass and radius observations imply tidal deformabilities for a 1.4 M_\odot NS between $(1.09 \text{ and } 2.12) \times 10^{36} \text{ g cm}^2 \text{ s}^2$ to 68% confidence over all four EOS models. These relatively small values may be challenging to measure in current GW observatories [7]. This result is a natural consequence of rather small neutron star radii implied by the qLMXBs [36, 37]. Over all four EOS models none of the 95% confidence limits goes higher than $2.6 \times 10^{36} \text{ g cm}^2 \text{ s}^2$.

As shown in Fig. 2, we find a strong correlation between the radius of a 1.4 M_\odot neutron star and the pressure at $\varepsilon = 300 \text{ MeV/fm}^3$ approximately twice the nuclear saturation density (lower-left panel). There is a

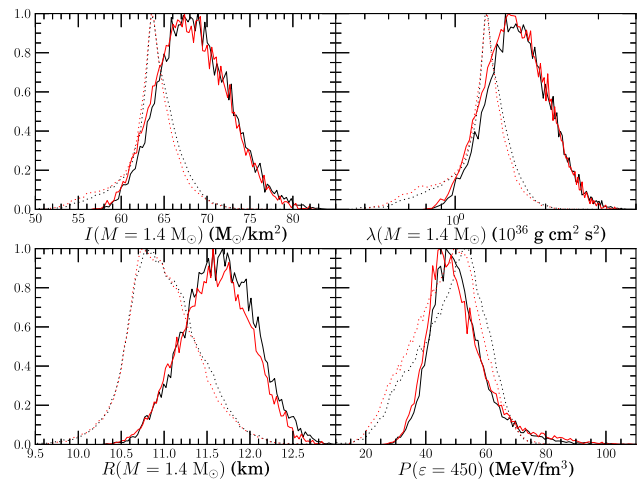


FIG. 1: Probability distributions for the moment of inertia of a 1.4 M_\odot NS (upper left), tidal deformability of a 1.4 M_\odot NS (upper right), radius of a 1.4 M_\odot NS (lower left) and pressure at about three times the saturation density (lower right) given the set of mass and radius observations. Black lines are for GCR and red lines are for HLPS. Solid lines are for Model A and dotted lines are for model C. Each of the distributions was separately normalized to have a maximum at 1.

slightly weaker, and more model-dependent, correlation between $\Delta I/I$ and the transition pressure (upper-left panel), and the correlation between $\Delta I/I$ and L is extremely weak (upper-right panel), as found in Ref. [28]. There is a significant range in crust thicknesses due to the EOS, even for a fixed mass and radius, as shown in the lower-right panel.

There is a quandary with pulsar glitches which originates in two results. The first is that some EOS models (like that of APR [55]) have small enough crusts that the fraction of the NS’s moment of inertia contained in the crust is somewhat small ($\Delta I/I < 0.05$ for a 1.4 M_\odot NS). The second is that there is a large amount of entrainment of superfluid neutrons by the lattice [56, 57], thus the amount of matter in the crust which is not strongly coupled to the lattice is only 15-25% of the total. Together, these limit the magnitude of pulsar glitches to be smaller than those already observed in the Vela pulsar which requires $\Delta I/I \geq 0.016$ [19, 20, 58]. As can be seen in the upper-right of Fig. 2, NS mass and radius data predict a similar outcome, and the quandary stands. If we assume, however, that systematic uncertainties invalidate current mass and radius observations (as implied by Ref. [59]) and use our third data set which only contains a measurement of the moment of inertia of $I = (70 \pm 7) M_\odot \text{ km}^2$, then we find many models with $\Delta I/I > 0.09$, as also shown in the upper-right panel. Smaller mass NSs give even larger values of $\Delta I/I$. We find that a measurement of $I = (90 \pm 9) M_\odot \text{ km}^2$ would imply that $\Delta I/I$ could be larger than 0.11. These large values of $\Delta I/I$ can accom-

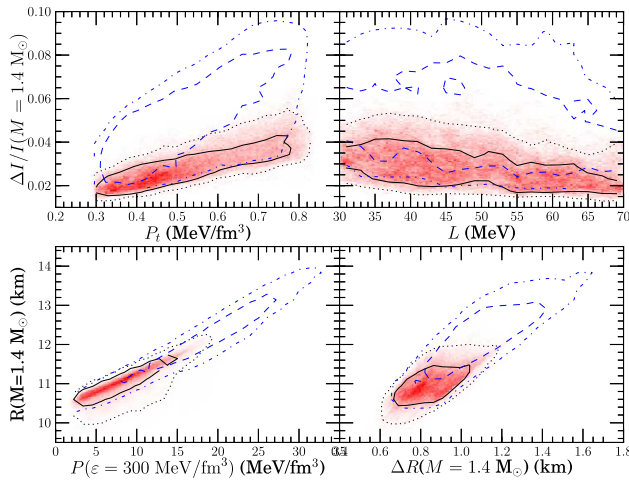


FIG. 2: Probability distributions for four pairs of quantities with EOS model GCR and Model C at high densities. In the upper-left panel, P_t is the pressure at the core-crust transition. All other quantities are defined in the text. The red density plot gives the probability distributions assuming the NS M and R data along with 68% contour lines (solid black) and 95% contour lines (dotted black). Also shown are the 68% (blue dashed) and 95% (blue dot-dashed) contour lines corresponding to the distribution given the third data set with only a measurement of $I = (70 \pm 7) M_\odot \text{ km}^2$.

moderate the observations of glitches in Vela even with the most extreme amounts of entrainment obtained in Ref. [56]. A similar conclusion has also been obtained independently in Ref. [60].

The thermal evolution of a NS crust as it cools depends on the hydrostatic structure of the crust (as well as on how photons and neutrons are transported). Frequently, crust cooling is studied using a small subset of the full variation possible for the hydrostatic structure [17, 18]. We find that, even for a fixed NS mass and radius, there is still considerable variation (due to the uncertainty in the EOS of dense matter) in the thickness of the crust. This is shown in the lower right panel of Fig. 2, where a histogram of the radius of a $1.4 M_\odot$ NS is plotted versus the crust thickness, ΔR . We find that, for a NS with an 11 km radius, the crust thickness varies by 42%. This means that a more complete variation of the parameter space may be required to determine the properties of the crust from crust cooling observations.

If a measurement of the moment of inertia of PSR J0737-3039A was far outside our predicted range, then that implies a conflict with the mass and radius observations. This conflict could be resolved with modification of strong-field GR. However, this modification may have to be finely tuned in order to modify the NS structure without spoiling the agreement with GR found in the observations of the post-Keplerian parameters in the PSR J0737-3039 system [61].

Current NS mass and radius observations are subject

to several strong systematic uncertainties (as described in Refs. [33, 34, 37]) and a moment of inertia measurement outside our predicted range could shed light on these systematics. Our understanding of NS structure would be best served by several different kinds of observations with different systematic uncertainties so that no one effect could dominate the results. The same reasoning given above also holds true for measurements of tidal deformabilities, crust thicknesses, and crustal fractions of the moment of inertia.

A large increase in the NS maximum mass, such as that implied by Refs. [62, 63], would significantly change these results. Larger maximum masses imply larger radii (larger pressure is needed at smaller densities in order to compete with gravity as the mass becomes larger), and thus larger moments of inertia and tidal deformabilities.

We thank C. Fryer, J.M. Lattimer, and S. Reddy for helpful discussions. A.W.S. is supported by DOE grant No. DE-FG02-00ER41132. S.G. is supported by DOE grants No. DE-AC02-05CH11231, by the NUCLEI SciDAC program, and by the LANL LDRD program. F.J.F. is supported by the NSF under grant No. PHY-1068022. F.J.F. and W.G.N. are supported by NASA through the Science Mission Directorate under grant No. NNX11AC41G. This research used resources of the National Energy Research Scientific Computing Center, which is supported by the Office of Science of the U.S. Department of Energy under Contract No. DE-AC02-05CH11231.

-
- [1] J. M. Lattimer and M. Prakash, *Astrophys. J.* **550**, 426 (2001).
 - [2] M. Burgay, N. D’Amico, A. Possenti, R. N. Manchester, A. G. Lyne, B. C. Joshi, M. A. McLaughlin, M. Kramer, J. M. Sarkissian, F. Camilo, et al., *Nature (London)* **426**, 531 (2003).
 - [3] M. Kramer, I. H. Stairs, R. N. Manchester, M. A. McLaughlin, A. G. Lyne, R. D. Ferdman, M. Burgay, D. R. Lorimer, A. Possenti, N. D’Amico, et al., *Science* **314**, 97 (2006).
 - [4] T. Damour and G. Schäfer, *Nuovo Cimento* **101**, 127 (1988).
 - [5] J. Abadie and et al., *Class. Quant. Grav.* **27**, 173001 (2010).
 - [6] E. Flanagan and T. Hinderer, *Phys. Rev. D* **77**, 021502 (2008).
 - [7] T. Hinderer, B. D. Lackey, R. N. Lang, and J. S. Read, *Phys. Rev. D* **81**, 123016 (2010).
 - [8] T. Damour, A. Nagar, and L. Villain, *Phys. Rev. D* **85**, 123007 (2012).
 - [9] W. Del Pozzo, T. G. F. Li, M. Agathos, C. Van Den Broeck, and S. Vitale, *Phys. Rev. Lett.* **111**, 071101 (2013).
 - [10] J. S. Read, L. Baiotti, J. D. E. Creighton, J. L. Friedman, B. Giacomazzo, K. Kyutoku, C. Markakis, L. Rezzolla, M. Shibata, and K. Taniguchi, *Phys. Rev. D* **88**, 044042 (2013).

- (2013).
- [11] K. Yagi and N. Yunes, *Science* **341**, 365 (2013).
 - [12] K. Yagi and N. Yunes, *Phys. Rev. D* **88**, 023009 (2013).
 - [13] J. M. Lattimer, K. A. van Riper, Madappa Prakash, and Manju Prakash, *Astrophys. J.* **425**, 802 (1994).
 - [14] R. E. Rutledge, L. Bildsten, E. F. Brown, G. G. Pavlov, V. E. Zavlin, and G. Ushomirsky, *Astrophys. J.* **580**, 413 (2002).
 - [15] W. H. G. Lewin and M. van der Klis, eds., *Compact Stellar X-Ray Sources* (Cambridge Univ. Press, Cambridge, England, 2006).
 - [16] P. S. Shternin, D. G. Yakolev, P. Haensel, and A. Y. Potekhin, *Mon. Not. R. Astron. Soc. Lett.* **382**, 43 (2007).
 - [17] E. F. Brown and A. Cumming, *Astrophys. J.* **698**, 1020 (2009).
 - [18] D. Page and S. Reddy, *Phys. Rev. Lett.* **111**, 241102 (2013).
 - [19] B. Link, R. I. Epstein, and J. M. Lattimer, *Phys. Rev. Lett.* **83**, 3362 (1999).
 - [20] N. Andersson, K. Glampedakis, W. C. G. Ho, and C. M. Espinoza, *Phys. Rev. Lett.* **109**, 241103 (2012).
 - [21] A. W. Steiner, M. Prakash, J. M. Lattimer, and P. J. Ellis, *Phys. Rep.* **411**, 325 (2005).
 - [22] B.-A. Li, A. Ramos, G. Verde, and I. Vidaña, *Eur. Phys. J. A* **50**, 1 (2014).
 - [23] A. W. Steiner, *Phys. Rev. C* **74**, 045808 (2006).
 - [24] V. Kalogera and D. Psaltis, *Phys. Rev. D* **61**, 024009 (1999).
 - [25] I. A. Morrison, T. W. Baumgarte, S. L. Shapiro, and V. R. Pandharipande, *Astrophys. J.* **617**, L135 (2004).
 - [26] M. Bejger, T. Bulik, and P. Haensel, *Mon. Not. R. Astron. Soc.* **364**, 635 (2005).
 - [27] J. M. Lattimer and B. F. Schutz, *Astrophys. J.* **629**, 979 (2005).
 - [28] F. J. Fattoyev and J. Piekarewicz, *Phys. Rev. C* **82**, 025810 (2010).
 - [29] F. J. Fattoyev, J. Carvajal, W. G. Newton, and B.-A. Li, *Phys. Rev. C* **87**, 015806 (2013).
 - [30] J. M. Lattimer and M. Prakash, *Phys. Rep.* **442**, 109 (2007).
 - [31] J. M. Lattimer and Y. Lim, *Astrophys. J.* **771**, 51 (2013).
 - [32] F. Özel, G. Baym, and T. Güver, *Phys. Rev. D* **82**, 101301 (2010).
 - [33] A. W. Steiner, J. M. Lattimer, and E. F. Brown, *Astrophys. J.* **770**, 1 (2010).
 - [34] A. W. Steiner, J. M. Lattimer, and E. F. Brown, *Astrophys. J. Lett.* **765**, 5 (2013).
 - [35] J. M. Lattimer and A. W. Steiner, *Eur. Phys. J. A* **50**, 40 (2014).
 - [36] S. Guillot, M. Servillat, N. A. Webb, and R. E. Rutledge, *Astrophys. J.* **772**, 7 (2013).
 - [37] J. M. Lattimer and A. W. Steiner, *Astrophys. J.* **784**, 123 (2014).
 - [38] W. E. Harris, *Astron. J.* **112**, 1487 (1996).
 - [39] P. Demorest, T. Pennucci, S. Ransom, M. Roberts, and J. W. T. Hessels, *Nature (London)* **467**, 1081 (2010).
 - [40] J. Antoniadis et al., *Science* **340**, 448 (2013).
 - [41] J. B. Hartle, *Astrophys. J.* **150**, 1005 (1967).
 - [42] J. B. Hartle and K. S. Thorne, *Astrophys. J.* **153**, 807 (1968).
 - [43] S. Postnikov, M. Prakash, and J. M. Lattimer, *Phys. Rev. D* **82**, 024016 (2010).
 - [44] S. Gandolfi, J. Carlson, and S. Reddy, *Phys. Rev. C* **85**, 032801(R) (2012).
 - [45] K. Hebeler, J. M. Lattimer, C. J. Pethick, and A. Schwenk, *Astrophys. J.* **773**, 11 (2013).
 - [46] M. Kortelainen, T. Lesinski, J. Moré, W. Nazarewicz, J. Sarich, N. Schunck, M. V. Stoitsov, and S. Wild, *Phys. Rev. C* **82**, 024313 (2010).
 - [47] A. W. Steiner and S. Gandolfi, *Phys. Rev. Lett.* **108**, 081102 (2012).
 - [48] I. Tews, T. Krüger, K. Hebeler, and A. Schwenk, *Phys. Rev. Lett.* **110**, 032504 (2013).
 - [49] S. Shlomo, V. Kolomietz, and G. Colò, *Eur. Phys. J. A* **30**, 23 (2006).
 - [50] J. Piekarewicz, *J. Phys. G* **37**, 064038 (2010).
 - [51] S. Gandolfi, J. Carlson, S. Reddy, A. W. Steiner, and R. B. Wiringa, *Eur. Phys. J. A* **50**, 1 (2014).
 - [52] P. Danielewicz and J. Lee, *Nucl. Phys. A* **922**, 1 (2014).
 - [53] W. G. Newton, M. Gearheart, and B.-A. Li, *Astrophys. J. Suppl.* **204**, 9 (2013).
 - [54] K. Oyamatsu and K. Iida, *Phys. Rev. C* **75**, 015801 (2007).
 - [55] A. Akmal, V. R. Pandharipande, and D. G. Ravenhall, *Phys. Rev. C* **58**, 1804 (1998).
 - [56] N. Chamel, *Nucl. Phys. A* **747**, 109 (2005).
 - [57] N. Chamel, *Phys. Rev. C* **85**, 035801 (2012).
 - [58] C. M. Espinoza, A. G. Lyne, B. W. Stappers, and M. Kramer, *Mon. Not. R. Astron. Soc.* **414**, 1679 (2011).
 - [59] V. Suleimanov, J. Poutanen, M. Revnivtsev, and K. Werner, *Astrophys. J.* **742**, 122 (2011).
 - [60] J. Piekarewicz, F. J. Fattoyev, and C. J. Horowitz, *in prep.* (2014).
 - [61] M. Kramer and N. Wex, *Class. Quant. Grav.* **26**, 073001 (2009).
 - [62] M. H. van Kerkwijk, R. P. Breton, and S. R. Kulkarni, *Astrophys. J.* **728**, 95 (2011).
 - [63] R. W. Romani, A. V. Filippenko, J. M. Silverman, S. B. Cenko, J. Greiner, A. Rau, J. Elliott, and H. J. Pletsch, *Astrophys. J. Lett.* **760**, L36 (2012).

Supplementary Material

Tables 1-12 give the 68% and 95% confidence limits for several physical parameters based on the associated marginal probability distributions for each of the 12 cases, 4 EOS models times 3 data sets. In addition, ≈ 100 independent points (separated as to remove auto-correlations) are included for each of these 12 data sets as text files. The text files are named first for the EOS model near saturation (“GCR” or “HLPS”), second for the high-density model (“A” or “C”) and third for the data set (“MR”, “MR_I70”, or “I70”). The columns for the text files are as follows:

1. “**mult**”: The relative multiplier, i.e. the number of times this point appeared in the chain
2. “**weight**”: Value of the likelihood function at this point
3. “**param_x**”: The EOS parameter values
4. “**P_x**”: The pressure (in MeV/fm³) at a specified energy density (in MeV/fm³)
5. “**L_V**”: The symmetry energy slope parameter (in MeV)
6. “**n_t**”: The core-crust transition density (in fm⁻³)
7. “**P_t**”: The core-crust transition pressure (in MeV/fm³)
8. “**Rc_x**”: The crust thickness (in km) of a neutron star of mass **x** (in M_\odot)
9. “**R_x**”: The radius (in km) of a neutron star of a mass **x** (in M_\odot)
10. “**I_x**”: The moment of inertia (in $M_\odot \text{ km}^2$) of a star of mass **x** (in M_\odot). The value “I.1.4” is not given for those data sets which include a measurement of I for J0737-3039A.
11. “**dI_x**”: The crustal fraction of the moment of inertia for a star of mass **x** (in M_\odot)
12. “**lam_x**”: The tidal deformability (in units of $10^{36} \text{ g cm}^2 \text{ s}^2$) for a star of mass **x** (in M_\odot)

In addition to the three data sets described in the paper, we also include four additional tables which present results with the GCR model assuming data sets of I measurements of $I = (80 \pm 8)$ or $(90 \pm 9) M_\odot \text{ km}^2$ and no mass and radius data.

Quantity (unit)	95% lower limit	68% lower limit	most probable	68% upper limit	95% upper limit
GCR + Model A + Mass and radius data					
$P(\varepsilon = 300)$ (MeV/fm ³)	9.318	13.31	16.91	19.72	22.86
$P(\varepsilon = 450)$ (MeV/fm ³)	33.31	40.98	47.07	57.40	71.02
$P(\varepsilon = 600)$ (MeV/fm ³)	90.98	103.7	125.8	141.1	160.8
$P(\varepsilon = 1000)$ (MeV/fm ³)	281.0	309.3	333.3	372.7	413.0
L (MeV)	30.53	39.30	47.74	57.38	65.79
n_t (fm ⁻³)	0.07142	0.07986	0.08502	0.09711	0.09903
P_t (MeV/fm ³)	0.3125	0.3180	0.4255	0.6973	0.8163
$\Delta R(n_t = 0.06, M = 1.4)$ (km)	0.6904	0.7657	0.8793	0.9408	1.037
$\Delta R(n_t = 0.08, M = 1.4)$ (km)	0.7455	0.8436	0.9386	1.099	1.206
$\Delta R(n_t = 0.10, M = 1.4)$ (km)	0.8025	0.9114	1.018	1.155	1.256
$\Delta R(n_t = 0.08, M = 1.0)$ (km)	1.164	1.312	1.448	1.699	1.881
$\Delta R(n_t = 0.08, M = 2.0)$ (km)	0.3411	0.3869	0.4427	0.5457	0.6475
$R(M = 1.4)$ (km)	10.79	11.26	11.67	12.11	12.44
$R(M = 1.7)$ (km)	10.74	11.12	11.49	11.93	12.40
$R(M = 2.0)$ (km)	10.16	10.62	11.09	11.67	12.25
R_{\max} (km)	9.812	10.19	10.77	11.08	11.57
$n_{B,\max}$ (fm ⁻³)	0.8770	0.9584	1.050	1.131	1.234
ε_{\max} (MeV/fm ³)	1055	1196	1292	1500	1597
$I(M = 1.4)$ (M _⊙ km ²)	60.62	64.15	68.93	72.37	77.06
$I(M = 1.7)$ (M _⊙ km ²)	80.11	84.17	88.90	95.39	101.5
$I(M = 2.0)$ (M _⊙ km ²)	94.49	100.8	107.6	116.9	126.7
$(\Delta I/I)(n_t = 0.08, M = 1.4)$	0.02045	0.02446	0.02897	0.04438	0.06084
$(\Delta I/I)(n_t = 0.08, M = 1.7)$	0.01284	0.01560	0.02019	0.02815	0.03703
$(\Delta I/I)(n_t = 0.08, M = 2.0)$	0.006949	0.008680	0.01169	0.01705	0.02317
$\lambda(M = 1.4)$ (10 ³⁶ g cm ² s ²)	1.000	1.264	1.476	2.124	2.606
$\lambda(M = 1.7)$ (10 ³⁶ g cm ² s ²)	0.6596	0.8480	1.159	1.502	2.067
$\lambda(M = 2.0)$ (10 ³⁶ g cm ² s ²)	0.2039	0.3202	0.5450	0.8213	1.276

Quantity (unit)	95% lower limit	68% lower limit	most probable	68% upper limit	95% upper limit
GCR + Model C + Mass and radius data					
$P(\varepsilon = 300)$ (MeV/fm ³)	2.253	3.332	5.767	10.89	15.83
$P(\varepsilon = 450)$ (MeV/fm ³)	25.88	39.87	52.71	62.18	68.09
$P(\varepsilon = 600)$ (MeV/fm ³)	76.56	137.0	196.3	209.1	216.3
$P(\varepsilon = 1000)$ (MeV/fm ³)	260.9	334.7	416.1	506.0	558.1
L (MeV)	30.53	33.18	41.89	60.63	68.41
n_t (fm ⁻³)	0.07168	0.07628	0.08906	0.09783	0.1021
P_t (MeV/fm ³)	0.3149	0.3274	0.4444	0.7669	0.7968
$\Delta R(n_t = 0.06, M = 1.4)$ (km)	0.5949	0.6529	0.7400	0.8192	0.9282
$\Delta R(n_t = 0.08, M = 1.4)$ (km)	0.6483	0.7183	0.8111	0.9511	1.088
$\Delta R(n_t = 0.10, M = 1.4)$ (km)	0.7073	0.7875	0.9221	1.005	1.136
$\Delta R(n_t = 0.08, M = 1.0)$ (km)	0.9457	1.046	1.255	1.399	1.651
$\Delta R(n_t = 0.08, M = 2.0)$ (km)	0.3252	0.4118	0.4840	0.5742	0.6401
$R(M = 1.4)$ (km)	10.22	10.56	10.80	11.34	11.87
$R(M = 1.7)$ (km)	10.31	10.81	11.05	11.55	11.95
$R(M = 2.0)$ (km)	10.10	10.86	11.30	11.76	12.01
R_{\max} (km)	9.792	10.34	11.04	11.42	11.81
$n_{B,\max}$ (fm ⁻³)	0.7642	0.8210	0.8617	1.066	1.235
ε_{\max} (MeV/fm ³)	578.4	952.3	988.1	1332	1612
$I(M = 1.4)$ (M _⊙ km ²)	56.25	61.67	63.60	66.74	69.87
$I(M = 1.7)$ (M _⊙ km ²)	77.02	85.89	89.48	93.24	95.49
$I(M = 2.0)$ (M _⊙ km ²)	97.59	109.9	119.1	123.3	125.0
$(\Delta I/I)(n_t = 0.08, M = 1.4)$	0.01555	0.01833	0.02483	0.03505	0.04723
$(\Delta I/I)(n_t = 0.08, M = 1.7)$	0.01033	0.01256	0.01764	0.02439	0.03211
$(\Delta I/I)(n_t = 0.08, M = 2.0)$	0.006129	0.008382	0.01180	0.01704	0.02231
$\lambda(M = 1.4)$ (10 ³⁶ g cm ² s ²)	0.7306	1.110	1.270	1.531	1.811
$\lambda(M = 1.7)$ (10 ³⁶ g cm ² s ²)	0.5258	0.9559	1.179	1.404	1.527
$\lambda(M = 2.0)$ (10 ³⁶ g cm ² s ²)	0.2635	0.5801	0.9789	1.140	1.211

Quantity (unit)	95% lower limit	68% lower limit	most probable	68% upper limit	95% upper limit
HLPS + Model A + Mass and radius data					
$P(\varepsilon = 300)$ (MeV/fm ³)	9.055	12.80	16.74	19.51	22.24
$P(\varepsilon = 450)$ (MeV/fm ³)	32.69	39.40	44.68	56.73	73.60
$P(\varepsilon = 600)$ (MeV/fm ³)	88.54	97.60	114.3	137.6	159.1
$P(\varepsilon = 1000)$ (MeV/fm ³)	283.6	314.8	341.1	377.2	412.7
L (MeV)	44.32	44.40	44.58	50.37	58.57
n_t (fm ⁻³)	0.07516	0.08055	0.08405	0.08802	0.09483
P_t (MeV/fm ³)	0.3441	0.3620	0.3842	0.4760	0.5972
$\Delta R(n_t = 0.06, M = 1.4)$ (km)	0.6454	0.7197	0.8007	0.8765	0.9591
$\Delta R(n_t = 0.08, M = 1.4)$ (km)	0.7307	0.8142	0.9179	1.014	1.123
$\Delta R(n_t = 0.10, M = 1.4)$ (km)	0.8231	0.9115	1.019	1.105	1.195
$\Delta R(n_t = 0.08, M = 1.0)$ (km)	1.142	1.266	1.470	1.585	1.763
$\Delta R(n_t = 0.08, M = 2.0)$ (km)	0.3167	0.3739	0.4250	0.5148	0.5906
$R(M = 1.4)$ (km)	10.82	11.22	11.57	12.05	12.42
$R(M = 1.7)$ (km)	10.70	11.03	11.56	11.97	12.33
$R(M = 2.0)$ (km)	10.06	10.51	11.13	11.62	12.21
R_{\max} (km)	9.744	10.09	10.76	10.98	11.47
$n_{B,\max}$ (fm ⁻³)	0.9165	1.017	1.073	1.207	1.277
ε_{\max} (MeV/fm ³)	1062	1215	1298	1512	1634
$I(M = 1.4)$ (M _⊙ km ²)	60.62	63.74	67.35	72.68	76.72
$I(M = 1.7)$ (M _⊙ km ²)	79.54	83.30	86.70	94.85	100.9
$I(M = 2.0)$ (M _⊙ km ²)	93.47	98.26	106.3	116.4	126.9
$(\Delta I/I)(n_t = 0.08, M = 1.4)$	0.02072	0.02450	0.03165	0.03690	0.04510
$(\Delta I/I)(n_t = 0.08, M = 1.7)$	0.01293	0.01551	0.02018	0.02316	0.02818
$(\Delta I/I)(n_t = 0.08, M = 2.0)$	0.006336	0.008359	0.01071	0.01391	0.01761
$\lambda(M = 1.4)$ (10 ³⁶ g cm ² s ²)	0.9919	1.231	1.510	2.051	2.570
$\lambda(M = 1.7)$ (10 ³⁶ g cm ² s ²)	0.6347	0.7757	1.021	1.476	1.968
$\lambda(M = 2.0)$ (10 ³⁶ g cm ² s ²)	0.1942	0.2712	0.5063	0.7705	1.285

Quantity (unit)	95% lower limit	68% lower limit	most probable	68% upper limit	95% upper limit
HLPS + Model C + Mass and radius data					
$P(\varepsilon = 300)$ (MeV/fm ³)	2.470	3.001	4.783	10.95	16.49
$P(\varepsilon = 450)$ (MeV/fm ³)	24.14	36.27	50.61	58.85	66.91
$P(\varepsilon = 600)$ (MeV/fm ³)	61.45	127.1	190.9	208.6	214.7
$P(\varepsilon = 1000)$ (MeV/fm ³)	266.7	340.5	417.0	501.0	560.0
L (MeV)	44.37	44.40	46.51	58.26	64.54
n_t (fm ⁻³)	0.07540	0.07849	0.08074	0.08927	0.09397
P_t (MeV/fm ³)	0.3406	0.3643	0.3935	0.5395	0.6061
$\Delta R(n_t = 0.06, M = 1.4)$ (km)	0.5714	0.6331	0.7010	0.7831	0.8867
$\Delta R(n_t = 0.08, M = 1.4)$ (km)	0.6457	0.7179	0.7999	0.9061	1.033
$\Delta R(n_t = 0.10, M = 1.4)$ (km)	0.7319	0.8023	0.9026	0.9848	1.115
$\Delta R(n_t = 0.08, M = 1.0)$ (km)	0.9416	1.039	1.196	1.356	1.591
$\Delta R(n_t = 0.08, M = 2.0)$ (km)	0.3056	0.4018	0.4602	0.5431	0.5947
$R(M = 1.4)$ (km)	10.21	10.56	10.74	11.31	11.86
$R(M = 1.7)$ (km)	10.25	10.78	11.05	11.51	11.91
$R(M = 2.0)$ (km)	9.961	10.74	11.26	11.69	11.97
R_{\max} (km)	9.550	10.20	10.89	11.30	11.65
$n_{B,\max}$ (fm ⁻³)	0.8014	0.8547	0.9369	1.121	1.274
ε_{\max} (MeV/fm ³)	914.3	962.5	1142	1417	1655
$I(M = 1.4)$ (M _⊙ km ²)	55.28	61.42	63.60	66.54	69.67
$I(M = 1.7)$ (M _⊙ km ²)	75.33	84.55	89.42	92.67	94.90
$I(M = 2.0)$ (M _⊙ km ²)	94.99	108.0	119.1	122.6	124.4
$(\Delta I/I)(n_t = 0.08, M = 1.4)$	0.01582	0.01935	0.02373	0.03060	0.03901
$(\Delta I/I)(n_t = 0.08, M = 1.7)$	0.01049	0.01321	0.01599	0.02084	0.02608
$(\Delta I/I)(n_t = 0.08, M = 2.0)$	0.005796	0.008587	0.01065	0.01443	0.01745
$\lambda(M = 1.4)$ (10 ³⁶ g cm ² s ²)	0.6511	1.085	1.273	1.508	1.750
$\lambda(M = 1.7)$ (10 ³⁶ g cm ² s ²)	0.4708	0.8749	1.177	1.354	1.488
$\lambda(M = 2.0)$ (10 ³⁶ g cm ² s ²)	0.2145	0.3127	0.9849	1.098	1.180

Quantity (unit)	95% lower limit	68% lower limit	most probable	68% upper limit	95% upper limit
	GCR + Model A + Mass and radius data + $I = 70$				
$P(\varepsilon = 300)$ (MeV/fm ³)	11.41	15.00	17.32	20.17	22.92
$P(\varepsilon = 450)$ (MeV/fm ³)	37.85	43.00	48.48	58.78	73.17
$P(\varepsilon = 600)$ (MeV/fm ³)	93.43	101.4	117.1	137.7	163.5
$P(\varepsilon = 1000)$ (MeV/fm ³)	274.4	308.2	338.9	377.7	420.9
L (MeV)	33.09	34.67	46.98	64.11	69.47
n_t (fm ⁻³)	0.07087	0.07330	0.08876	0.09900	0.1006
P_t (MeV/fm ³)	0.3014	0.3064	0.3822	0.7777	0.8005
$\Delta R(n_t = 0.06, M = 1.4)$ (km)	0.7197	0.7733	0.8354	0.9587	1.085
$\Delta R(n_t = 0.08, M = 1.4)$ (km)	0.7740	0.8323	0.9202	1.122	1.269
$\Delta R(n_t = 0.10, M = 1.4)$ (km)	0.8505	0.9231	1.031	1.190	1.320
$\Delta R(n_t = 0.08, M = 1.0)$ (km)	1.202	1.297	1.404	1.747	1.923
$\Delta R(n_t = 0.08, M = 2.0)$ (km)	0.3303	0.3803	0.4420	0.5662	0.6724
$R(M = 1.4)$ (km)	11.12	11.40	11.82	12.14	12.57
$R(M = 1.7)$ (km)	10.95	11.23	11.65	12.01	12.48
$R(M = 2.0)$ (km)	10.30	10.74	11.20	11.78	12.30
R_{\max} (km)	9.982	10.26	10.74	11.10	11.76
$n_{B,\max}$ (fm ⁻³)	0.8577	0.9466	1.060	1.149	1.213
ε_{\max} (MeV/fm ³)	1027	1195	1285	1499	1567
$I(M = 1.7)$ (M _⊙ km ²)	82.01	85.64	89.13	96.16	102.3
$I(M = 2.0)$ (M _⊙ km ²)	96.41	101.9	107.9	119.4	128.1
$(\Delta I/I)(n_t = 0.08, M = 1.4)$	0.02464	0.02675	0.03066	0.05458	0.06823
$(\Delta I/I)(n_t = 0.08, M = 1.7)$	0.01353	0.01490	0.01820	0.03262	0.04022
$(\Delta I/I)(n_t = 0.08, M = 2.0)$	0.006761	0.007945	0.01047	0.01838	0.02528
$\lambda(M = 1.4)$ (10 ³⁶ g cm ² s ²)	0.8879	1.097	1.380	1.698	2.106
$\lambda(M = 1.7)$ (10 ³⁶ g cm ² s ²)	0.7533	0.9096	1.162	1.617	2.133
$\lambda(M = 2.0)$ (10 ³⁶ g cm ² s ²)	0.2269	0.3334	0.5649	0.8667	1.376

Quantity (unit)	95% lower limit	68% lower limit	most probable	68% upper limit	95% upper limit
	GCR + Model C + Mass and radius data + $I = 70$				
$P(\varepsilon = 300)$ (MeV/fm ³)	2.640	4.954	9.687	13.56	17.58
$P(\varepsilon = 450)$ (MeV/fm ³)	33.69	43.11	52.38	62.73	70.46
$P(\varepsilon = 600)$ (MeV/fm ³)	102.6	147.8	196.8	209.9	218.4
$P(\varepsilon = 1000)$ (MeV/fm ³)	264.9	334.5	395.6	535.6	575.3
L (MeV)	30.57	34.39	49.00	58.11	67.27
n_t (fm ⁻³)	0.07170	0.07619	0.09081	0.09576	0.1019
P_t (MeV/fm ³)	0.3280	0.3395	0.3923	0.7621	0.7961
$\Delta R(n_t = 0.06, M = 1.4)$ (km)	0.6255	0.6801	0.7611	0.8581	0.9725
$\Delta R(n_t = 0.08, M = 1.4)$ (km)	0.6766	0.7444	0.8671	0.9900	1.152
$\Delta R(n_t = 0.10, M = 1.4)$ (km)	0.7468	0.8152	0.9305	1.054	1.191
$\Delta R(n_t = 0.08, M = 1.0)$ (km)	0.9714	1.088	1.248	1.491	1.764
$\Delta R(n_t = 0.08, M = 2.0)$ (km)	0.3643	0.4278	0.5155	0.5844	0.6668
$R(M = 1.4)$ (km)	10.47	10.73	11.18	11.56	12.03
$R(M = 1.7)$ (km)	10.66	10.94	11.27	11.66	12.07
$R(M = 2.0)$ (km)	10.49	11.04	11.39	11.82	12.14
R_{\max} (km)	10.02	10.52	11.10	11.44	11.89
$n_{B,\max}$ (fm ⁻³)	0.7658	0.8171	0.9196	1.022	1.196
ε_{\max} (MeV/fm ³)	879.7	957.1	1209	1303	1574
$I(M = 1.7)$ (M _⊙ km ²)	81.86	87.11	89.69	93.48	96.66
$I(M = 2.0)$ (M _⊙ km ²)	102.7	113.2	119.6	123.6	126.3
$(\Delta I/I)(n_t = 0.08, M = 1.4)$	0.01814	0.02158	0.02880	0.04194	0.05774
$(\Delta I/I)(n_t = 0.08, M = 1.7)$	0.01153	0.01338	0.01496	0.02590	0.03512
$(\Delta I/I)(n_t = 0.08, M = 2.0)$	0.007329	0.009041	0.01308	0.01799	0.02404
$\lambda(M = 1.4)$ (10 ³⁶ g cm ² s ²)	0.7065	0.8394	0.9421	1.165	1.489
$\lambda(M = 1.7)$ (10 ³⁶ g cm ² s ²)	0.7502	1.028	1.180	1.426	1.644
$\lambda(M = 2.0)$ (10 ³⁶ g cm ² s ²)	0.3868	0.7254	1.005	1.170	1.292

Quantity (unit)	95% lower limit	68% lower limit	most probable	68% upper limit	95% upper limit
HLPS + Model A + Mass and radius data + $I = 70$					
$P(\varepsilon = 300)$ (MeV/fm ³)	11.59	16.02	18.07	20.35	22.86
$P(\varepsilon = 450)$ (MeV/fm ³)	38.43	43.65	50.33	57.78	73.47
$P(\varepsilon = 600)$ (MeV/fm ³)	93.44	100.7	118.3	134.7	160.3
$P(\varepsilon = 1000)$ (MeV/fm ³)	281.3	309.4	347.2	378.6	419.3
L (MeV)	44.32	44.43	46.42	50.69	58.86
n_t (fm ⁻³)	0.07758	0.08020	0.08478	0.09128	0.09417
P_t (MeV/fm ³)	0.3514	0.3659	0.4463	0.5263	0.6041
$\Delta R(n_t = 0.06, M = 1.4)$ (km)	0.7080	0.7678	0.8426	0.9291	1.015
$\Delta R(n_t = 0.08, M = 1.4)$ (km)	0.8011	0.8728	0.9847	1.074	1.188
$\Delta R(n_t = 0.10, M = 1.4)$ (km)	0.8987	0.9841	1.054	1.169	1.252
$\Delta R(n_t = 0.08, M = 1.0)$ (km)	1.258	1.377	1.461	1.702	1.814
$\Delta R(n_t = 0.08, M = 2.0)$ (km)	0.3392	0.3996	0.4788	0.5500	0.6441
$R(M = 1.4)$ (km)	11.13	11.51	11.86	12.16	12.49
$R(M = 1.7)$ (km)	10.99	11.31	11.64	12.05	12.47
$R(M = 2.0)$ (km)	10.27	10.73	11.19	11.76	12.30
R_{\max} (km)	9.947	10.24	10.78	11.14	11.64
$n_{B,\max}$ (fm ⁻³)	0.8898	0.9706	1.069	1.142	1.237
ε_{\max} (MeV/fm ³)	1040	1184	1282	1496	1594
$I(M = 1.7)$ (M _⊙ km ²)	82.25	85.82	90.60	96.09	101.9
$I(M = 2.0)$ (M _⊙ km ²)	96.04	101.5	109.6	117.5	127.8
$(\Delta I/I)(n_t = 0.08, M = 1.4)$	0.02693	0.03087	0.03952	0.04586	0.05400
$(\Delta I/I)(n_t = 0.08, M = 1.7)$	0.01479	0.01692	0.02309	0.02578	0.03214
$(\Delta I/I)(n_t = 0.08, M = 2.0)$	0.007185	0.009061	0.01247	0.01566	0.02061
$\lambda(M = 1.4)$ (10 ³⁶ g cm ² s ²)	0.9285	1.155	1.385	1.714	2.096
$\lambda(M = 1.7)$ (10 ³⁶ g cm ² s ²)	0.7568	0.9268	1.243	1.566	2.089
$\lambda(M = 2.0)$ (10 ³⁶ g cm ² s ²)	0.2282	0.3361	0.5328	0.8512	1.336

Quantity (unit)	95% lower limit	68% lower limit	most probable	68% upper limit	95% upper limit
HLPS + Model C + Mass and radius data + $I = 70$					
$P(\varepsilon = 300)$ (MeV/fm ³)	2.608	4.530	8.960	13.81	17.62
$P(\varepsilon = 450)$ (MeV/fm ³)	32.95	44.38	55.21	63.58	70.99
$P(\varepsilon = 600)$ (MeV/fm ³)	97.91	151.2	198.4	211.9	218.9
$P(\varepsilon = 1000)$ (MeV/fm ³)	252.2	272.7	377.7	460.6	563.3
L (MeV)	44.42	44.44	44.95	59.47	64.55
n_t (fm ⁻³)	0.07324	0.07554	0.08384	0.08847	0.09362
P_t (MeV/fm ³)	0.3270	0.3445	0.3740	0.5904	0.6043
$\Delta R(n_t = 0.06, M = 1.4)$ (km)	0.5987	0.6530	0.7296	0.8166	0.9177
$\Delta R(n_t = 0.08, M = 1.4)$ (km)	0.6739	0.7397	0.8486	0.9431	1.067
$\Delta R(n_t = 0.10, M = 1.4)$ (km)	0.7722	0.8415	0.9347	1.042	1.168
$\Delta R(n_t = 0.08, M = 1.0)$ (km)	0.9562	1.061	1.219	1.423	1.656
$\Delta R(n_t = 0.08, M = 2.0)$ (km)	0.3551	0.4298	0.4814	0.5573	0.6227
$R(M = 1.4)$ (km)	10.50	10.69	11.21	11.57	12.09
$R(M = 1.7)$ (km)	10.67	10.95	11.33	11.68	12.15
$R(M = 2.0)$ (km)	10.44	11.07	11.37	11.87	12.22
R_{\max} (km)	9.947	10.56	11.21	11.59	11.94
$n_{B,\max}$ (fm ⁻³)	0.7628	0.8313	0.8848	1.058	1.232
ε_{\max} (MeV/fm ³)	578.5	959.9	998.0	1300	1566
$I(M = 1.7)$ (M _⊙ km ²)	81.34	87.50	89.86	93.70	97.51
$I(M = 2.0)$ (M _⊙ km ²)	101.4	113.8	119.5	124.3	127.3
$(\Delta I/I)(n_t = 0.08, M = 1.4)$	0.01774	0.02143	0.02893	0.03577	0.04588
$(\Delta I/I)(n_t = 0.08, M = 1.7)$	0.01142	0.01372	0.01665	0.02202	0.02754
$(\Delta I/I)(n_t = 0.08, M = 2.0)$	0.007179	0.009382	0.01144	0.01520	0.01907
$\lambda(M = 1.4)$ (10 ³⁶ g cm ² s ²)	0.6982	0.8446	0.9283	1.182	1.547
$\lambda(M = 1.7)$ (10 ³⁶ g cm ² s ²)	0.7086	1.051	1.197	1.442	1.687
$\lambda(M = 2.0)$ (10 ³⁶ g cm ² s ²)	0.3430	0.7396	0.9955	1.203	1.327

Quantity (unit)	95% lower limit	68% lower limit	most probable	68% upper limit	95% upper limit
GCR + Model A + $I = 70$ only					
$P(\varepsilon = 300)$ (MeV/fm ³)	14.51	18.57	22.03	27.81	39.05
$P(\varepsilon = 450)$ (MeV/fm ³)	44.51	50.61	60.56	80.46	106.2
$P(\varepsilon = 600)$ (MeV/fm ³)	102.1	113.7	134.6	158.6	191.8
$P(\varepsilon = 1000)$ (MeV/fm ³)	258.8	279.5	310.9	384.7	439.6
L (MeV)	33.36	47.27	53.10	69.44	69.61
n_t (fm ⁻³)	0.07134	0.07493	0.07731	0.09065	0.1010
P_t (MeV/fm ³)	0.3363	0.3966	0.5115	0.7501	0.7944
$\Delta R(n_t = 0.06, M = 1.4)$ (km)	0.8428	0.9354	1.095	1.175	1.312
$\Delta R(n_t = 0.08, M = 1.4)$ (km)	0.9200	1.033	1.217	1.355	1.533
$\Delta R(n_t = 0.10, M = 1.4)$ (km)	1.000	1.148	1.288	1.495	1.659
$\Delta R(n_t = 0.08, M = 1.0)$ (km)	1.421	1.611	1.868	2.071	2.234
$\Delta R(n_t = 0.08, M = 2.0)$ (km)	0.4194	0.5052	0.6114	0.7578	0.9220
$R(M = 1.4)$ (km)	11.66	12.15	12.59	13.16	13.67
$R(M = 1.7)$ (km)	11.44	11.99	12.56	13.15	13.72
$R(M = 2.0)$ (km)	10.83	11.52	12.22	13.05	13.79
R_{\max} (km)	10.36	10.85	11.62	12.21	13.03
$n_{B,\max}$ (fm ⁻³)	0.6758	0.7943	0.9001	1.040	1.112
ε_{\max} (MeV/fm ³)	780.1	963.2	1051	1304	1440
$I(M = 1.7)$ (M _⊙ km ²)	86.73	93.75	100.4	111.0	120.4
$I(M = 2.0)$ (M _⊙ km ²)	101.3	111.3	125.4	139.0	153.3
$(\Delta I/I)(n_t = 0.08, M = 1.4)$	0.03228	0.04011	0.05285	0.07382	0.08882
$(\Delta I/I)(n_t = 0.08, M = 1.7)$	0.01812	0.02320	0.03293	0.04339	0.05649
$(\Delta I/I)(n_t = 0.08, M = 2.0)$	0.009625	0.01342	0.02013	0.02790	0.03913
$\lambda(M = 1.4)$ (10 ³⁶ g cm ² s ²)	1.186	1.595	2.011	2.815	3.710
$\lambda(M = 1.7)$ (10 ³⁶ g cm ² s ²)	0.9348	1.283	1.887	2.821	4.089
$\lambda(M = 2.0)$ (10 ³⁶ g cm ² s ²)	0.2926	0.5027	0.9031	1.826	3.167

Quantity (unit)	95% lower limit	68% lower limit	most probable	68% upper limit	95% upper limit
GCR + Model C + $I = 70$ only					
$P(\varepsilon = 300)$ (MeV/fm ³)	3.821	14.21	21.80	26.44	28.80
$P(\varepsilon = 450)$ (MeV/fm ³)	37.76	51.21	62.65	79.08	86.87
$P(\varepsilon = 600)$ (MeV/fm ³)	86.68	146.2	201.1	223.6	237.0
$P(\varepsilon = 1000)$ (MeV/fm ³)	261.6	280.2	408.2	508.3	564.1
L (MeV)	30.55	31.55	55.02	63.10	67.16
n_t (fm ⁻³)	0.07149	0.07643	0.08484	0.09576	0.1013
P_t (MeV/fm ³)	0.3228	0.3439	0.3814	0.6855	0.7932
$\Delta R(n_t = 0.06, M = 1.4)$ (km)	0.6521	0.7885	0.9716	1.127	1.262
$\Delta R(n_t = 0.08, M = 1.4)$ (km)	0.7091	0.8700	1.096	1.290	1.477
$\Delta R(n_t = 0.10, M = 1.4)$ (km)	0.7821	0.9539	1.159	1.388	1.560
$\Delta R(n_t = 0.08, M = 1.0)$ (km)	1.074	1.334	1.734	2.141	2.343
$\Delta R(n_t = 0.08, M = 2.0)$ (km)	0.3847	0.4769	0.5868	0.7091	0.8156
$R(M = 1.4)$ (km)	10.55	11.51	12.47	13.06	13.47
$R(M = 1.7)$ (km)	10.78	11.53	12.41	12.85	13.24
$R(M = 2.0)$ (km)	10.58	11.45	12.38	12.75	13.12
R_{\max} (km)	10.11	10.92	11.75	12.38	12.66
$n_{B,\max}$ (fm ⁻³)	0.6871	0.7428	0.8212	1.007	1.181
ε_{\max} (MeV/fm ³)	575.5	898.4	989.5	1272	1571
$I(M = 1.7)$ (M _⊙ km ²)	81.79	89.07	99.73	103.3	110.5
$I(M = 2.0)$ (M _⊙ km ²)	100.7	116.5	126.4	133.5	138.8
$(\Delta I/I)(n_t = 0.08, M = 1.4)$	0.01961	0.02849	0.04181	0.06716	0.08703
$(\Delta I/I)(n_t = 0.08, M = 1.7)$	0.01262	0.01709	0.02332	0.03763	0.05081
$(\Delta I/I)(n_t = 0.08, M = 2.0)$	0.008142	0.01036	0.01495	0.02384	0.03370
$\lambda(M = 1.4)$ (10 ³⁶ g cm ² s ²)	0.6954	0.8408	0.9801	2.179	3.568
$\lambda(M = 1.7)$ (10 ³⁶ g cm ² s ²)	0.6982	1.087	1.290	2.151	2.849
$\lambda(M = 2.0)$ (10 ³⁶ g cm ² s ²)	0.2817	0.8099	1.131	1.685	1.965

Quantity (unit)	95% lower limit	68% lower limit	most probable	68% upper limit	95% upper limit
HLPS + Model A + $I = 70$ only					
$P(\varepsilon = 300)$ (MeV/fm ³)	15.66	17.88	20.99	27.07	39.14
$P(\varepsilon = 450)$ (MeV/fm ³)	44.18	49.90	59.34	84.38	108.6
$P(\varepsilon = 600)$ (MeV/fm ³)	102.4	114.6	130.4	161.2	194.0
$P(\varepsilon = 1000)$ (MeV/fm ³)	257.6	280.8	340.8	392.0	441.1
L (MeV)	44.38	44.45	46.59	55.35	63.13
n_t (fm ⁻³)	0.07366	0.07867	0.08140	0.08825	0.09211
P_t (MeV/fm ³)	0.3237	0.3462	0.3815	0.5016	0.5921
$\Delta R(n_t = 0.06, M = 1.4)$ (km)	0.7876	0.8713	0.9517	1.072	1.187
$\Delta R(n_t = 0.08, M = 1.4)$ (km)	0.8889	0.9731	1.072	1.221	1.382
$\Delta R(n_t = 0.10, M = 1.4)$ (km)	1.003	1.101	1.227	1.352	1.489
$\Delta R(n_t = 0.08, M = 1.0)$ (km)	1.393	1.489	1.570	1.798	2.013
$\Delta R(n_t = 0.08, M = 2.0)$ (km)	0.3958	0.4798	0.5941	0.7124	0.8440
$R(M = 1.4)$ (km)	11.66	12.07	12.58	13.01	13.43
$R(M = 1.7)$ (km)	11.42	11.86	12.55	13.11	13.59
$R(M = 2.0)$ (km)	10.79	11.52	12.25	13.09	13.72
R_{\max} (km)	10.35	10.81	11.74	12.31	13.04
$n_{B,\max}$ (fm ⁻³)	0.6846	0.7791	0.9063	1.057	1.138
ε_{\max} (MeV/fm ³)	775.1	906.1	1063	1292	1420
$I(M = 1.7)$ (M _⊙ km ²)	86.35	92.98	101.1	111.1	120.7
$I(M = 2.0)$ (M _⊙ km ²)	101.7	112.5	126.4	140.6	153.7
$(\Delta I/I)(n_t = 0.08, M = 1.4)$	0.03146	0.03580	0.04257	0.05344	0.06573
$(\Delta I/I)(n_t = 0.08, M = 1.7)$	0.01704	0.02073	0.02618	0.03321	0.04234
$(\Delta I/I)(n_t = 0.08, M = 2.0)$	0.008696	0.01189	0.01700	0.02231	0.02986
$\lambda(M = 1.4)$ (10 ³⁶ g cm ² s ²)	1.225	1.522	1.954	2.750	3.545
$\lambda(M = 1.7)$ (10 ³⁶ g cm ² s ²)	0.9210	1.254	2.058	2.824	4.009
$\lambda(M = 2.0)$ (10 ³⁶ g cm ² s ²)	0.2889	0.4760	0.8868	2.022	3.169

Quantity (unit)	95% lower limit	68% lower limit	most probable	68% upper limit	95% upper limit
HLPS + Model C + $I = 70$ only					
$P(\varepsilon = 300)$ (MeV/fm ³)	3.120	14.24	21.60	25.78	29.71
$P(\varepsilon = 450)$ (MeV/fm ³)	36.47	47.73	64.15	76.25	87.49
$P(\varepsilon = 600)$ (MeV/fm ³)	81.47	135.3	197.5	223.6	236.1
$P(\varepsilon = 1000)$ (MeV/fm ³)	270.5	359.3	455.3	515.1	568.3
L (MeV)	44.40	44.46	45.69	58.62	64.54
n_t (fm ⁻³)	0.07486	0.07875	0.08410	0.08882	0.09341
P_t (MeV/fm ³)	0.3410	0.3749	0.3894	0.5831	0.6060
$\Delta R(n_t = 0.06, M = 1.4)$ (km)	0.6482	0.7584	0.9325	1.090	1.232
$\Delta R(n_t = 0.08, M = 1.4)$ (km)	0.7399	0.8618	1.089	1.266	1.430
$\Delta R(n_t = 0.10, M = 1.4)$ (km)	0.8214	1.001	1.176	1.370	1.560
$\Delta R(n_t = 0.08, M = 1.0)$ (km)	1.115	1.442	1.710	2.046	2.208
$\Delta R(n_t = 0.08, M = 2.0)$ (km)	0.3793	0.4701	0.5944	0.6764	0.7748
$R(M = 1.4)$ (km)	10.64	11.51	12.29	12.96	13.64
$R(M = 1.7)$ (km)	10.81	11.53	12.17	12.79	13.34
$R(M = 2.0)$ (km)	10.58	11.38	12.09	12.69	13.13
R_{\max} (km)	10.16	10.76	11.30	12.04	12.61
$n_{B,\max}$ (fm ⁻³)	0.7171	0.7703	0.8350	1.008	1.177
ε_{\max} (MeV/fm ³)	579.7	927.1	977.2	1260	1544
$I(M = 1.7)$ (M _⊙ km ²)	80.38	88.87	96.67	103.0	111.3
$I(M = 2.0)$ (M _⊙ km ²)	100.2	114.8	125.3	133.1	138.6
$(\Delta I/I)(n_t = 0.08, M = 1.4)$	0.02214	0.02977	0.04420	0.06055	0.07244
$(\Delta I/I)(n_t = 0.08, M = 1.7)$	0.01331	0.01821	0.02557	0.03326	0.04192
$(\Delta I/I)(n_t = 0.08, M = 2.0)$	0.007985	0.01126	0.01715	0.02135	0.02756
$\lambda(M = 1.4)$ (10 ³⁶ g cm ² s ²)	0.6406	0.8610	1.550	2.187	3.918
$\lambda(M = 1.7)$ (10 ³⁶ g cm ² s ²)	0.6156	1.085	1.673	2.135	2.924
$\lambda(M = 2.0)$ (10 ³⁶ g cm ² s ²)	0.2909	0.7261	1.250	1.640	1.996

Quantity (unit)	95% lower limit	68% lower limit	most probable	68% upper limit	95% upper limit
	GCR + Model A + $I = 80$ only				
$P(\varepsilon = 300)$ (MeV/fm ³)	17.55	20.66	26.99	37.77	57.00
$P(\varepsilon = 450)$ (MeV/fm ³)	54.30	64.10	80.90	100.7	125.1
$P(\varepsilon = 600)$ (MeV/fm ³)	108.3	116.0	133.1	173.0	208.4
$P(\varepsilon = 1000)$ (MeV/fm ³)	259.1	271.6	310.7	391.9	457.9
L (MeV)	35.10	41.30	51.39	65.96	67.95
n_t (fm ⁻³)	0.07130	0.07781	0.07915	0.09162	0.1017
P_t (MeV/fm ³)	0.3252	0.3519	0.4675	0.6387	0.7881
$\Delta R(n_t = 0.06, M = 1.4)$ (km)	0.8987	0.9936	1.155	1.268	1.433
$\Delta R(n_t = 0.08, M = 1.4)$ (km)	0.9798	1.087	1.264	1.474	1.671
$\Delta R(n_t = 0.10, M = 1.4)$ (km)	1.057	1.190	1.369	1.585	1.790
$\Delta R(n_t = 0.08, M = 1.0)$ (km)	1.475	1.628	1.746	2.123	2.331
$\Delta R(n_t = 0.08, M = 2.0)$ (km)	0.4792	0.5989	0.7583	0.9006	1.071
$R(M = 1.4)$ (km)	12.04	12.58	13.00	13.67	14.14
$R(M = 1.7)$ (km)	11.93	12.57	13.14	13.86	14.35
$R(M = 2.0)$ (km)	11.43	12.26	13.08	13.92	14.61
R_{\max} (km)	10.82	11.38	12.21	13.11	13.93
$n_{B,\max}$ (fm ⁻³)	0.6107	0.6744	0.7954	0.9032	1.037
ε_{\max} (MeV/fm ³)	694.2	784.1	926.6	1106	1310
$I(M = 1.7)$ (M _⊙ km ²)	93.98	102.3	114.6	122.9	132.8
$I(M = 2.0)$ (M _⊙ km ²)	110.7	124.7	142.6	157.7	172.2
$(\Delta I/I)(n_t = 0.08, M = 1.4)$	0.03595	0.04094	0.04998	0.07755	0.09641
$(\Delta I/I)(n_t = 0.08, M = 1.7)$	0.02122	0.02594	0.03356	0.04947	0.06618
$(\Delta I/I)(n_t = 0.08, M = 2.0)$	0.01200	0.01596	0.02299	0.03408	0.04914
$\lambda(M = 1.4)$ (10 ³⁶ g cm ² s ²)	1.548	2.037	2.607	4.007	4.875
$\lambda(M = 1.7)$ (10 ³⁶ g cm ² s ²)	1.325	1.869	2.795	4.303	5.922
$\lambda(M = 2.0)$ (10 ³⁶ g cm ² s ²)	0.4620	0.9273	1.735	3.243	5.222

Quantity (unit)	95% lower limit	68% lower limit	most probable	68% upper limit	95% upper limit
GCR + Model C + $I = 80$ only					
$P(\varepsilon = 300)$ (MeV/fm ³)	12.03	20.81	26.31	34.33	40.44
$P(\varepsilon = 450)$ (MeV/fm ³)	47.11	61.80	69.33	88.09	100.5
$P(\varepsilon = 600)$ (MeV/fm ³)	95.07	147.0	204.0	227.9	243.0
$P(\varepsilon = 1000)$ (MeV/fm ³)	264.8	320.2	412.4	508.3	580.9
L (MeV)	30.34	30.59	42.99	52.17	66.00
n_t (fm ⁻³)	0.07406	0.08303	0.08630	0.09947	0.1028
P_t (MeV/fm ³)	0.3388	0.3821	0.6742	0.7773	0.8132
$\Delta R(n_t = 0.06, M = 1.4)$ (km)	0.7839	1.014	1.159	1.398	1.514
$\Delta R(n_t = 0.08, M = 1.4)$ (km)	0.8970	1.140	1.294	1.632	1.784
$\Delta R(n_t = 0.10, M = 1.4)$ (km)	0.9163	1.209	1.368	1.693	1.841
$\Delta R(n_t = 0.08, M = 1.0)$ (km)	1.365	1.813	1.900	2.395	2.541
$\Delta R(n_t = 0.08, M = 2.0)$ (km)	0.4683	0.5904	0.7107	0.8590	1.005
$R(M = 1.4)$ (km)	11.36	12.62	14.04	14.21	14.41
$R(M = 1.7)$ (km)	11.46	12.21	12.98	13.80	14.47
$R(M = 2.0)$ (km)	11.20	11.99	12.74	13.44	14.19
R_{\max} (km)	10.41	11.43	12.52	12.88	13.42
$n_{B,\max}$ (fm ⁻³)	0.6212	0.6958	0.7827	0.9081	1.093
ε_{\max} (MeV/fm ³)	568.1	580.2	987.1	1171	1458
$I(M = 1.7)$ (M _⊙ km ²)	89.25	93.84	107.5	117.6	133.2
$I(M = 2.0)$ (M _⊙ km ²)	105.3	121.2	132.6	143.3	158.6
$(\Delta I/I)(n_t = 0.08, M = 1.4)$	0.03190	0.04954	0.05732	0.09607	0.1095
$(\Delta I/I)(n_t = 0.08, M = 1.7)$	0.01784	0.02631	0.03489	0.05450	0.06909
$(\Delta I/I)(n_t = 0.08, M = 2.0)$	0.009485	0.01630	0.02345	0.03449	0.04472
$\lambda(M = 1.4)$ (10 ³⁶ g cm ² s ²)	0.9336	1.496	2.456	4.828	5.604
$\lambda(M = 1.7)$ (10 ³⁶ g cm ² s ²)	0.7341	1.263	2.282	3.355	6.058
$\lambda(M = 2.0)$ (10 ³⁶ g cm ² s ²)	0.3238	0.9344	1.655	2.319	3.506

Quantity (unit)	95% lower limit	68% lower limit	most probable	68% upper limit	95% upper limit
GCR + Model A + $I = 90$ only					
$P(\varepsilon = 300)$ (MeV/fm ³)	20.39	24.08	36.62	49.50	65.70
$P(\varepsilon = 450)$ (MeV/fm ³)	60.53	67.99	81.73	106.7	132.1
$P(\varepsilon = 600)$ (MeV/fm ³)	104.6	114.1	131.5	177.9	220.3
$P(\varepsilon = 1000)$ (MeV/fm ³)	260.4	270.2	309.5	418.5	461.2
L (MeV)	35.64	41.03	56.27	69.49	69.66
n_t (fm ⁻³)	0.07061	0.07225	0.08193	0.09514	0.09766
P_t (MeV/fm ³)	0.3119	0.3228	0.4087	0.6255	0.8006
$\Delta R(n_t = 0.06, M = 1.4)$ (km)	0.9550	1.079	1.183	1.358	1.488
$\Delta R(n_t = 0.08, M = 1.4)$ (km)	1.038	1.159	1.328	1.546	1.729
$\Delta R(n_t = 0.10, M = 1.4)$ (km)	1.136	1.297	1.500	1.684	1.863
$\Delta R(n_t = 0.08, M = 1.0)$ (km)	1.539	1.686	2.023	2.180	2.383
$\Delta R(n_t = 0.08, M = 2.0)$ (km)	0.5420	0.6732	0.8660	0.9936	1.154
$R(M = 1.4)$ (km)	12.39	12.96	13.61	14.15	14.47
$R(M = 1.7)$ (km)	12.36	13.04	13.88	14.43	14.82
$R(M = 2.0)$ (km)	11.96	12.92	13.65	14.62	15.13
R_{\max} (km)	11.15	11.91	13.01	13.75	14.49
$n_{B,\max}$ (fm ⁻³)	0.6059	0.6124	0.7014	0.8097	0.9794
ε_{\max} (MeV/fm ³)	624.7	694.3	831.9	1048	1236
$I(M = 1.7)$ (M _⊙ km ²)	99.06	109.9	120.7	133.9	141.5
$I(M = 2.0)$ (M _⊙ km ²)	119.3	136.7	150.4	172.3	184.4
$(\Delta I/I)(n_t = 0.08, M = 1.4)$	0.03895	0.04380	0.05610	0.07995	0.1033
$(\Delta I/I)(n_t = 0.08, M = 1.7)$	0.02346	0.02877	0.04012	0.05491	0.07233
$(\Delta I/I)(n_t = 0.08, M = 2.0)$	0.01377	0.01970	0.03084	0.04005	0.05424
$\lambda(M = 1.4)$ (10 ³⁶ g cm ² s ²)	1.945	2.659	3.790	4.836	5.904
$\lambda(M = 1.7)$ (10 ³⁶ g cm ² s ²)	1.716	2.630	4.009	5.935	7.505
$\lambda(M = 2.0)$ (10 ³⁶ g cm ² s ²)	0.6898	1.327	3.088	4.676	6.865

Quantity (unit)	95% lower limit	68% lower limit	most probable	68% upper limit	95% upper limit
GCR + Model C + $I = 90$ only					
$P(\varepsilon = 300)$ (MeV/fm ³)	4.401	26.29	32.05	40.14	41.71
$P(\varepsilon = 450)$ (MeV/fm ³)	50.96	62.78	80.63	93.69	105.1
$P(\varepsilon = 600)$ (MeV/fm ³)	95.46	144.0	203.9	236.7	252.5
$P(\varepsilon = 1000)$ (MeV/fm ³)	260.6	274.8	411.8	465.2	559.7
L (MeV)	30.46	33.78	50.10	60.39	66.43
n_t (fm ⁻³)	0.07315	0.07938	0.08360	0.09637	0.1003
P_t (MeV/fm ³)	0.3364	0.3675	0.4519	0.6847	0.7869
$\Delta R(n_t = 0.06, M = 1.4)$ (km)	0.6661	1.089	1.266	1.474	1.599
$\Delta R(n_t = 0.08, M = 1.4)$ (km)	0.8744	1.213	1.409	1.718	1.866
$\Delta R(n_t = 0.10, M = 1.4)$ (km)	0.8213	1.249	1.475	1.778	2.040
$\Delta R(n_t = 0.08, M = 1.0)$ (km)	1.064	1.803	1.963	2.454	2.614
$\Delta R(n_t = 0.08, M = 2.0)$ (km)	0.4422	0.6272	0.7664	0.9263	1.039
$R(M = 1.4)$ (km)	10.59	13.24	14.11	14.52	14.68
$R(M = 1.7)$ (km)	11.02	12.87	13.91	14.50	14.73
$R(M = 2.0)$ (km)	11.21	12.48	13.16	14.13	14.38
R_{\max} (km)	10.58	11.66	12.84	13.11	13.44
$n_{B,\max}$ (fm ⁻³)	0.6111	0.6762	0.7628	0.8728	1.103
ε_{\max} (MeV/fm ³)	564.5	574.2	988.0	1119	1475
$I(M = 1.7)$ (M _⊙ km ²)	89.26	105.4	111.8	133.9	135.7
$I(M = 2.0)$ (M _⊙ km ²)	111.6	121.9	139.1	151.4	164.9
$(\Delta I/I)(n_t = 0.08, M = 1.4)$	0.03230	0.04769	0.06023	0.1066	0.1173
$(\Delta I/I)(n_t = 0.08, M = 1.7)$	0.01547	0.02683	0.04129	0.05852	0.07652
$(\Delta I/I)(n_t = 0.08, M = 2.0)$	0.009756	0.01677	0.02481	0.03816	0.04921
$\lambda(M = 1.4)$ (10 ³⁶ g cm ² s ²)	0.8586	0.8756	5.006	5.951	6.142
$\lambda(M = 1.7)$ (10 ³⁶ g cm ² s ²)	1.090	1.150	3.086	4.520	6.484
$\lambda(M = 2.0)$ (10 ³⁶ g cm ² s ²)	0.4520	0.9309	2.183	2.873	4.246